ISSN 0018-151X, High Temperature, 2016, Vol. 54, No. 5, pp. 690–697. © Pleiades Publishing, Ltd., 2016.
Original Russian Text © A.E. Galashev, 2016, published in Teplofizika Vysokikh Temperatur, 2016, Vol. 54, No. 5, pp. 733–741.

THERMOPHYSICAL PROPERTIES OF MATERIALS

Molecular-Dynamic Analysis of Fast Heating of a Mercury Film on Graphene

A. E. Galashev

Institute of High-Temperature Electrochemistry, Ural Branch, Russian Academy of Sciences,
Yekaterinburg, 620137 Russia
e-mail: galashev@ihte.uran.ru

Received January 23, 2015

Abstract—Stepwise heating of a mercury film on graphene with Stone–Wales defects and hydrogenated edges is studied by the molecular dynamics methods at 800 K. Transformation of the film into a drop and its detachment from graphene is observed at a temperature of ~700 K. The phonon spectra determined by horizontal and vertical atomic vibrations, the mobility coefficients of Hg atoms separated in directions, the density profile and radial distribution function of mercury, the angular distribution of nearest geometrical neighbors, the stress tensor of graphene, and the roughness of a graphene sheet are calculated.

DOI: 10.1134/S0018151X16050102

INTRODUCTION

Due to recently discovered unique electronic, mechanical, and thermal properties, single-layer graphene is considered a promising material and the methods developed for its synthesis make possible various applications [1]. However, the use of graphene as an anode material and as anti-corrosion coating does not always give positive results because of the chemical instability induced by some fluids. A hazard for graphene is posed, e.g., by aqueous solution of an electrolyte (six-mol LiCl) [2]. In the zone where graphene placed on a SiO_2 substrate preliminarily treated by oxygen plasma made contact with a liquid drop of this solution, a rupture of the graphene sheet was observed. Washing in acetone and isopropyl alcohol and covering the graphene with methyl methacrylate before applying it onto a SiO_2 substrate instead of oxygen plasma treatment made it possible to reduce to some extent (up to 70%) the number of disruptions of graphene and evaporation of drops [3]. In [2, 3], the main reason for the disruption of graphene flakes was specified as the action of a contacting liquid on it and the transfer of the stress from the substrate to flakes was pointed out. This conclusion was based on the fact that two-layer graphene subjected to similar treatment is substantially more stable for contact with the same drops and, as a rule, is not disrupted. A possible reason for the destruction of graphene in both the first (with oxygen plasma treatment) and second (without plasma treatment) cases may be the formation of COOH groups on the graphene sheet surface. Oxygen bound to graphene captures hydrogen from adsorbed molecules (water, isopropyl alcohol, etc.); i.e., a reaction with release of a large amount of energy proceeds:

$$H_2 + 1/2O_2 = H_2O + 285.75 \text{ kJ/mol}. \qquad (1)$$

This energy is quite sufficient for the local heating of the surface to $T = 873$ K and initiating the reaction

$$C + H_2O + 131.25 \text{ kJ/mol} = CO + H_2,$$

which leads to the destruction of graphene and filling the near-surface region with hydrogen and CO gas. The newly arriving hydrogen goes to the maintenance of reaction (1). The stability of graphene in the presence of a liquid drop on its surface requires intensive study, because such contact can lead to catastrophic consequences.

In [4, 5], various samples of C absorbing Hg in the simulation of coal combustion and stack gas formation were studied. X-ray absorption fine structure (XAFS) spectroscopy was applied. The XAFS spectra indicated chemosorption of Hg on C. On the basis of these data, it may be assumed that the adsorption process is due to the halogenide, sulfide, and oxygen anions present on the C surface. In addition, in [6], by X-ray adsorption spectroscopy and X-ray photoelectron spectroscopy, after the exposure of carbon samples to stack gases containing Hg (204 μg/m^3), chlorinated and bromated activated carbon was found. On the activated carbon surface, no Hg was found but Hg–Br and Hg–Cl complexes were present. This result gave foundation to the assumption that the capture of Hg by chlorinated and bromated activated carbon is reached through the surface oxidation of Hg, followed by adsorption.

In [7], the mechanism of bounding mercury by sorbents from activated carbon was studied. It was shown that, at low Hg concentrations, the oxidation and adsorption mechanisms are hardly distinguishable. The difference between them gradually increases with the Hg concentration and the enhancement of the Hg–Hg interaction. However, since HgO, Hg_2Br_2, and $HgBr_2$ have close binding energies, these surface-bound compounds, as a rule, are not distinguished by photoelectron spectroscopy.

Recently, graphene membranes began to be employed in filters for detecting minute amounts of undesirable impurities [8, 9]. The multiple exploitation of graphene in filters requires its nondestructive cleaning from adsorbed substances. Cleaning graphene from metals can be performed by exposing it to a cluster beam of noble gases [10] or by heating [11, 12]. However, heating should be used in the cases when the metal has a sufficiently low boiling point T_b. One such metal is mercury. Ideal graphene, as a rule, is not destroyed upon heating it to the boiling points of many metals, such as Al, Ni, and Cu, although, in this case, its edges are damaged [11–13]. Graphene edges can be strengthened by hydrogenation. Such graphene endures cluster bombardment even at a beam energy of 30 eV [10]. It is not clear what will be the behavior of graphene with a high concentration of Stone–Wales defects, because it is these defects that form before its melting [14].

The aim of the present work is to study the possibility to remove mercury from graphene hydrogenated on the edges and having a high concentration of Stone–Wales defects by heating to a temperature above T_b of metal.

COMPUTER MODEL

Interatomic interactions in graphene are described by the modified many-body Tersoff potential [15]. The energy of pairwise interaction of atoms *i* and *j* with allowance for the influence of other atoms (multiparticle effects) is written as

$$V_{ij} = f_C(r_{ij})\left[A\exp(-\lambda^{(1)}r_{ij}) - Bb_{ij}\exp(-\lambda^{(2)}r_{ij})\right],$$

$$f_C(r_{ij}) = \begin{cases} 1, & r_{ij} < R^{(1)} \\ \frac{1}{2} + \frac{1}{2}\cos\left[\pi\left(r_{ij} - R^{(1)}\right)\big/(R^{(2)} - R^{(1)})\right], & R^{(1)} < r_{ij} < R^{(2)}, \\ 0 & r_{ij} > R^{(2)} \end{cases}$$

where r_{ij} is the distance between atoms *i* and *j* the parameters *A* and *B* specify the energy characteristics of repulsion and attraction, b_{ij} is the many-body bond-order parameter, describing the creation of the bond energy (the attractive part V_{ij}) in a local atom arrangement due to the presence of other neighboring atoms. The parameters $R^{(1)}$ and $R^{(2)}$ are chosen so that only the nearest neighbors are involved. The potential energy is a many-body function of the positions of atoms *i*, *j*, and *k* and is determined by the parameters

$$b_{ij} = (1 + \beta^n\xi_{ij}^{n_i})^{-1/(2n)}, \quad \xi_{ij} = \sum_{k\neq i,j} f_C(r_{ij})g(\theta_{ijk}),$$
$$g(\theta_{ijk}) = 1 + \frac{c^2}{d^2} - \frac{c^2}{\left[d^2 + (h - \cos\theta_{ijk})^2\right]}, \qquad (2)$$

where the parameters n, n_i, and β specifying the bonding force are functions of the environment; ξ_{ij} is the effective coordination number, determining the average number of nearest neighbors with allowance of not only the distances between them but also the bond angle θ_{ijk}; $g(\theta_{ijk})$ is the function of the angle between $\mathbf{r}_{ij}$ and $\mathbf{r}_{ik}$; $\mathbf{r}_{ij}$ is the vector issuing from the position of the atom *i* to the point where atom *j* is located; *d* establishes the width of the sharp peak in the angular dependence $g(\theta_{ijk})$; *c* specifies the height of this peak; $g(\theta_{ijk})$ has a minimum at $h = \cos(\theta)$. The summation in (2) is performed over all *k* neighbors of the first order. Such neighbors are chosen for each *i*–*j* pair and are defined at each instant of time. All parameters of the potential were chosen so as to match the theoretical and experimental data (the cohesion energy, lattice parameters, bulk moduli) for real and hypothetic graphite and diamond.

Due to insufficiently accurate determination of the force characteristics establishing the C–C bond, the Tersoff potential has no barrier for the rotation about a single bond. The inadequacy of the semi-empirical Tersoff potential, which was revealed in the study of the dynamic properties of graphite and manifests itself in the rotation of the entire simulated fragment, is corrected by adding to it the torsion potential [16]. The parameters of this potential were refined by matching the observed properties (mean-square deviations for the vibration frequencies) of graphite and diamond. The new analytical form of the local torsion potential is presented in [17]. In that work, the use of weights for bonds provides a smooth removal of the energy of torsion connected with the dihedral angle in any successive disruption of bonds [17]. The covalence bonding in the original Tersoff potential was bounded by r_b = 0.21 nm. The simulation of graphene by this potential led not only to uncontrolled rotation but also to cracking of the graphene sheet [18]. In this connection, in this work, r_b was increased to 0.23 nm and an additional weak attraction for $r > 0.23$ nm, specified by an additional Lennard–Jones (LD) potential with the parameters from [17], was introduced.

In the present work, the Hg–Hg interactions were determined by means of the potential proposed by Schwerdtfeger (Sch-potential) for simulating the dimer Hg_2 [19]. The Sch-potential for the simulation of liquid mercury is based on *ab initio* calculations and has the form

$$V_{\mathrm{Sch}}(r) = U_{\mathrm{Sch}}(\lambda r) = \sum_{j=3}^{9} a_{2j}^{*} r^{-2j}. \qquad (3)$$

The authors of [20] scaled the distances by the factor $\lambda = 1.167$. The parameters a_{2j}^{*} presented in [20] correspond to liquid Hg at $T = 300$ K. The pair Sch-potential (3) reproduces the basic properties of mercury, such as the melting point and density of liquid Hg, sufficiently well.

Calculations were also performed with the Silvera–Goldman potential (SG-potential) [21]:

$$V_{\mathrm{SG}}(r) = \exp(\alpha - \beta r - \gamma r^2) - f_c(r)\left(\sum_{n=3}^{5} \frac{C_{2n}}{r^{2n}}\right),$$

where the function switching over the interaction upon reaching the distance r_c is represented in the form

$$f_c(r) = \begin{cases} \exp\left[-(r_c/r - 1)^2\right], & r < r_c \\ 1.0, & r \ge r_c \end{cases}.$$

The parameters of this potential are presented in [21].

Defects substantially enhance the adhesion of metals by graphene. One of the most widely occurring defects in graphene is the Stone–Wales (SW) defect, which consist of connected carbon rings with five or seven atoms, arising due to the rotation by 90° of neighboring carbon atoms about their center. The graphene sheet used here for deposition of mercury had six such defects distributed approximately uniformly over its surface.

Graphene edges were strengthened by hydrogenation. The real maximum adsorption of hydrogen by graphene proceeds at a pressure of 1 MPa in the form of physisorption; one hydrogen atom is accommodated by one carbon atom of the adsorbing surface. The doping of graphene with Pd atoms favors formation of the CH-group [22]. CH-groups forming on the edges of the sheet were simulated by the one-atom scheme [22]. The C–CH and CH–CH interactions were represented by the LD potential. The partial functionalization of graphene in the form of the attachment of hydrogen atoms to its edges stabilizes the structure without increasing the interatomic distances and without creating roughness of the entire surface.

The mercury film on graphene was formed in a separate molecular-dynamic (MD) computation in two stages. At the first stage, Hg atoms were placed over the center of nonadjacent graphene cells so that the distance between Hg and C atoms was 2.30 Å (calculated from the density functional theory [7]). Onto this loose film, consisting of 49 Hg atoms, 51 more Hg atoms were deposited in a random manner. Then this system, consisting of 100 Hg atoms and 406 C atoms, was brought to equilibrium in an MD computation involving 10^6 time steps ($\Delta t = 0.2$ fs). These equations of motion were solved numerically by the Verlet algorithm [23]. The target obtained in this way was subjected to stepwise heating, which consisted of raising the temperature by 100 K from the previous state. The final configuration of the previous computation was used as the initial configuration for the new state.

The temperature in the system was maintained by the Berendsen scheme with the coupling constant $\tau = 4$ fs [24]. At each time step, the atom velocities v were scaled as

$$v = \lambda v, \quad \lambda = \left[1 + \frac{\Delta t}{\tau}\left(\frac{T_0}{T} - 1\right)\right]^{1/2},$$

where λ is the scaling factor, T_0 is the specified initial temperature (300 K), and T is the current temperature.

The self-diffusion coefficient was determined in terms of the mean squared displacement of Hg atoms as

$$D = D_{xy} + D_z = \frac{1}{2\Gamma\tau}\left\langle [\Delta \mathbf{r}(t)]^2 \right\rangle_p,$$

where $\Gamma = 3$ is the dimension of space. Angular brackets denote averaging with respect to the number of time intervals p necessary for determining $\left\langle [\Delta \mathbf{r}(t)]^2 \right\rangle$. The averaging of five time dependences, each calculated in the interval of $t = 200$ ps, is performed.

The metal film density profile was calculated as

$$\rho(z) = \frac{n(z)\delta_{\mathrm{Hg}}^3}{\Delta h S_{xy} N_s},$$

where $n(z)$ is the number of Hg atoms in a layer parallel to the graphene plane, δ_{Hg} is the effective diameter of the Hg atom; Δh is the layer thickness; S_{xy} is the graphene surface area; and N_s is the number of tests.

For calculating the stresses arising in graphene, the graphene sheet was divided into elementary areas. The stresses $\sigma_{u\alpha}(l)$ on an elementary area with the orientation marked by the index u and order number l for each of the directions x, y, and z designated by the current index α are determined by calculating the product of the projections of the atomic velocities on this area and by the projections of forces f_{ij}^{α}, acting upon the lth area from other atoms under the corresponding conditions [25]:

$$\sigma_{u\alpha}(l) = \left\langle \sum_{i}^{k} \frac{1}{\Omega}\left(m v_u^i v_\alpha^i\right) \right\rangle + \frac{1}{S_l}\left\langle \sum_{i}^{k} \sum_{j \ne i}^{(u_i \le u, u_j \ge u)} \left(f_{ij}^{\alpha}\right) \right\rangle,$$

where k is the number of atoms on the lth area; Ω is the volume per atom; m is the atomic mass; v_α^i is the α-projection of the velocity of atom i; S_l is the area of the lth area; the force arising on the interaction of atoms i and j passes through the lth area; and u_i is the current coor-

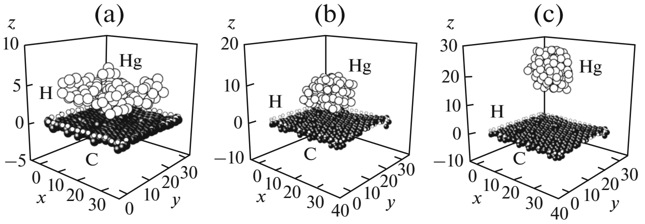

Fig. 1. Configuration of the Hg film on partly hydrogenated graphene, obtained by stepwise heating at the temperature of (a) 300, (b) 600, and (c) 1100 K; coordinates are expressed in angstroms.

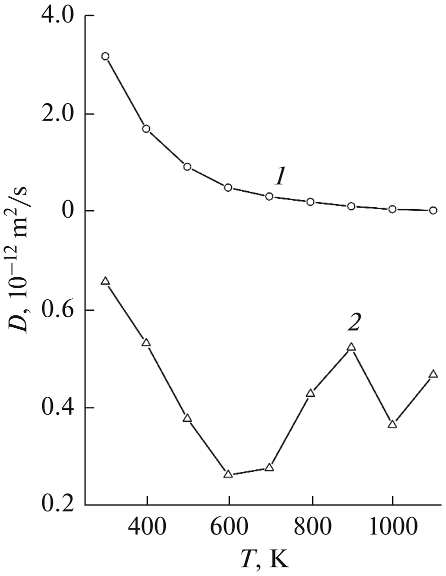

Fig. 2. Coefficients of (*1*) horizontal and (*2*) vertical mobility of Hg atoms, obtained on heating of liquid mercury on graphene.

dinate of atom *i*, where *u* can take the values *x*, *y*, and *z*. If $u = z$, *u* is the average level of C atoms in graphene.

The graphene sheet had sizes of 3.4 × 2.8 nm. Each *l*th area separated in this sheet and extended along the axis *oy* (in the perpendicular "zigzag" direction of graphene) contained 14 C atoms and had an area of 0.68 nm^2. The total stresses acting in the graphene plane were determined by the summation of the corresponding elementary stresses:

$$\sigma_{u\alpha} = \sum_{l=1}^{N_l} \sigma_{u\alpha}(l),$$

where N_l is the number of elementary areas.

The surface roughness (or the mean absolute deviation of the profile) was calculated as

$$R_a = \frac{1}{N}\sum_{i=1}^{N} |z_i - \overline{z}|,$$

where N is the number of nodes (atoms) on the graphene surface, z_i is the level of atom *i*, and $\overline{z}$ is the level of the graphene surface; the quantities z_i and $\overline{z}$ are determined at the same time.

The total energy of free single-sheet graphene at $T = 300$ K was found to be–7.02 eV, which agrees with the quantum mechanical calculation (–6.98 eV) [26]. The isochoric heat capacity of liquid mercury at this temperature calculated by the MD model, 28.4 J/mol K, agrees with the experimental value of 26.9 J/mol K.

COMPUTATIONAL RESULTS

Taking into account the time step, the computation duration, and the temperature increment, it is easy to evaluate the average heating rate of the system by ~10^{11} K/s. In these conditions, if there is no total structural relaxation of the system, the system can be overheated. In the case of metals, the overheating increases due to the influence of the electron subsystem, which stabilized the condensed state. The changes observed upon heating the mercury film on graphene are shown in Fig. 1. The liquid-metal film begins detachment from graphene already at $T = 300$ K. This phenomenon manifests itself in raising the film edge over graphene. Atoms of the middle part of the curved Hg film are still connected with the substrate; the minimum distance $r_{\mathrm{C-Hg}}^{\min}$ between some Hg atoms and C atoms is 0.31 nm. At the temperature of 600 K, the Hg film completely transforms into a drop that has not lost its connection with graphene. The distance $r_{\mathrm{C-Hg}}^{\min}$ in this case reaches 0.36 nm. A further increase in temperature leads to the detachment of the drop from the graphene surface, and, at the temperature of 1100 K, $r_{\mathrm{C-Hg}}^{\min}$ becomes large (1.55 nm).

Along with the transformation of the Hg film into a drop with the subsequent detachment of the drop from the substrate, the horizontal component D_{xy} of the mobility of mercury atoms decreases and the vertical component D_z, after a fast decrease, on approaching the temperature of 600 K, nonmonotonically increases again (Fig. 2). A smooth decrease in D_{xy} characterizes the transformation of the film into a drop and densification of the drop with increasing distance from graphene. The behavior of D_z indicates that the drop formation process terminates at $T = 600$ K, and, with a further increase in temperature, the oscillatory process of raising the drop over the graphene surface takes place.

How strongly the vibrational oscillatory spectra of Hg atoms are transformed as the temperature increases from 300 to 1100 K is demonstrated by Fig. 3. The spectrum of horizontal vibrations at $T = 300$ K is characterized by strong bursts, which decrease with frequency. At 1100 K, the asymptotics of this spectrum has not changed but the intensity of decreasing peaks has decreased by a factor of six to seven. The spectrum of vertical vibrations gradually reduces its intensity and com-

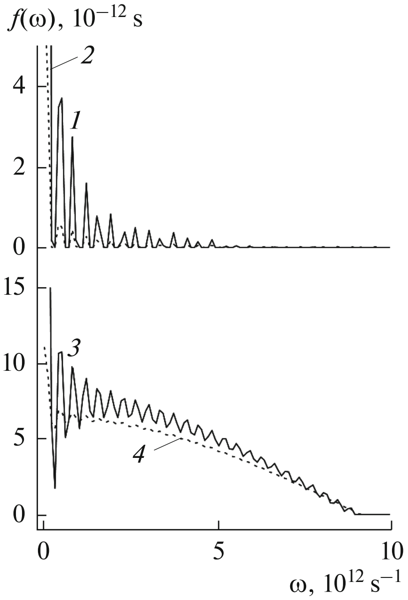

Fig. 3. Horizontal (*1*, *2*) and (*3*, *4*) vertical components of the phonon spectrum of liquid mercury on graphene, obtained at the temperatures of (*1*, *3*) 300 and (*2*, *4*) 1100 K.

pletely vanishes at the frequencies $\omega \geq 8.9 \times 10^{12}$ s^{-1}, regardless of temperature. However, with an increase in temperature, small-scale vibrations imposed onto the contour of the spectrum are smoothed out. The spectrum of vertical vibrations has an appreciably wider domain than the spectrum of horizontal vibrations of Hg atoms.

The vertical profiles $\rho(z)$ of the density of mercury at the temperatures of 300 and 800 K are presented in Fig. 4. The narrow profile $\rho(z)$ at $T = 300$ K has two sharp peaks indicating the dominantly two-layer arrangement of Hg atoms on graphene. However, at $T = 800$ K, the density profile expands and shifts upward. The low intensity of the spectrum $\rho(z)$ on the edges and the large density of intense peaks in the middle of the spectrum indicate the formation of a spheroidal formation: a drop. The influence of the substrate manifests itself in the formation of a layered structure of the drop, which is indicated by a large number of narrow peaks in the spectrum of $\rho(z)$. The very close mutual arrangement of a series of such peaks evidences the irregularity of the forming structure.

The radial distribution functions $g(r)$ constructed for Hg atoms nearest to the center of mass of liquid mercury also clearly evidences the formation of a more compact structure at $T = 1100$ K than at the initial temperature (Fig. 5). The function $g(r)$ reflects the spherically averaged structure of liquid mercury, including that in the horizontal plane, which is not given by the function $\rho(z)$. The contraction and widening of the peaks of $g(r)$ at $T = 1100$ K evidences the formation of an irregular compact structure in which the distance to the first-order neighbors is estimated as $r_1 = 0.29$ nm and the distance to the second-order neighbors, as $r_2 = 0.60$ nm. The experimental values of these quantities for liquid mercury at the temperature of 300 K are $r_1 = 0.31$ nm and $r_2 = 0.59$ nm [27].

In the angular distribution of the nearest neighbors in graphene at $T = 300$ K, the peak at 120° dominates, which indicates the presence of the basic elements of a two-dimensional structure: hexagonal cells (Fig. 6). The additional peaks in this distribution are formed due to the high density of Stone–Wales defects (pentagonal and heptagonal cells). Although the temperature of 1100 K is not high for graphene (its melting point is $T_m = 4900$ K), its structure has suffered noticeable changes. The peak at 120° has become

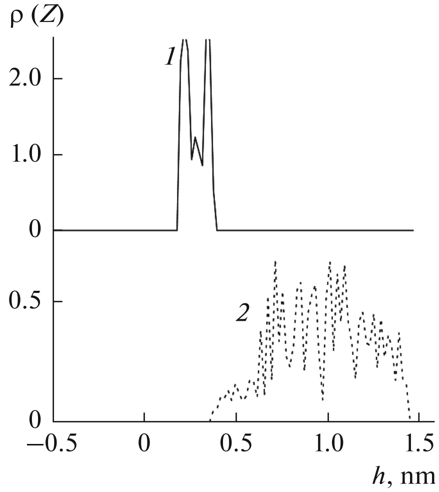

Fig. 4. Vertical profiles of the density of liquid mercury on graphene at the temperatures of (*1*) 300 and (*2*) 800 K.

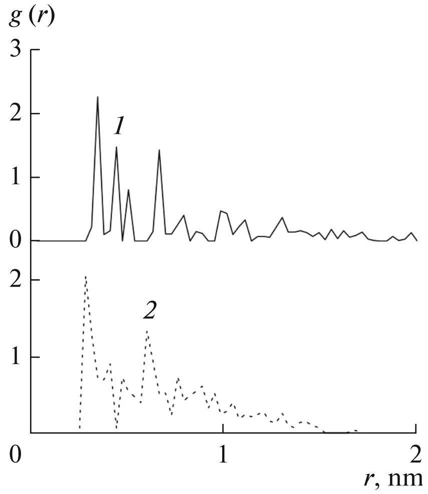

Fig. 5. Radial distribution functions of liquid mercury on graphene, calculated at the temperatures of (*1*) 300 and (*2*) 1100 K.

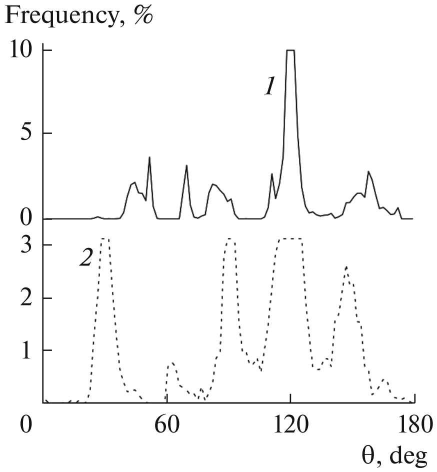

Fig. 6. Angular distributions for nearest neighbors in graphene with a high concentration of Stone–Wales defects, corresponding to the temperatures of (*1*) 300 and (*2*) 1100 K.

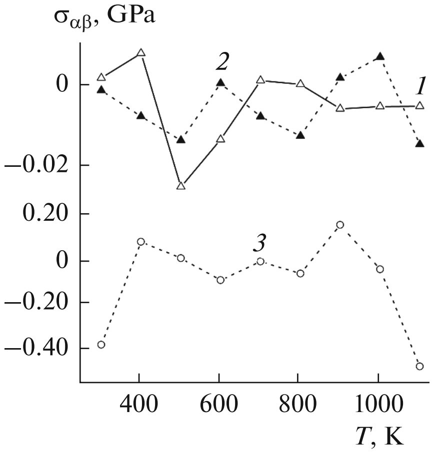

Fig. 7. Temperature dependence of stresses (*1*) σ_{zx}, (*2*) σ_{zy}, and (*3*) σ_{zz} acting in the plane of a graphene sheet with defects covered with mercury.

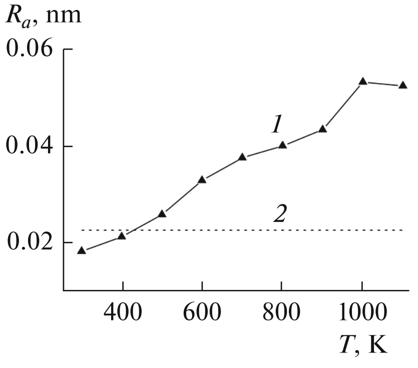

Fig. 8. The roughness of graphene covered with mercury (*1*) under the action of heating and (2) subjected to the bombardment with Xe_{13} clusters with an energy of 30 eV.

appreciably wider. In addition, the peaks at 30°, 90°, and 150° have significantly increased their intensities. These changes indicate the growth of defects in the graphene structure.

The stresses (σ_{zx} and σ_{zy}) characterizing the action of internal horizontal forces in the graphene plane vary insignificantly with temperature (Fig. 7). The stress σ_{zx} tends to a slight increase, while σ_{zy} decreases nonmonotonically, starting from 500 K. The stress σ_{zz}, which characterizes the action of vertical forces, exceeds σ_{zx} and σ_{zy} by more than an order of magnitude. The function $|\sigma_{zz}(T)|$ has two sections of fastest variation: a decrease with heating to 400 K and an increase with an increase in temperature begining from 900 K. The minimum of $|\sigma_{zz}|$ is reached at 700 K, when the mercury drop, having formed, detaches from the graphene.

Figure 8 presents a comparison of the temperature dependence $R_a(T)$ of the roughness of graphene having six Stone–Wales defects with the R_a of a graphene sheet of the same sizes but containing nine monovacancies and subjected to cluster bombardment. In both cases, graphene originally has a mercury cover of 100 atoms. The roughness R_a of graphene full with Stone–Wales defects increases rapidly with temperature. In the case of the vertical bombardment with Hg clusters with an energy of 30 eV, the vacancy-containing graphene acquired roughness that can be assigned to the temperature of ~400 K for the first case. The strong binding between C atoms in graphene is preserved also at a high temperature, as a result of which the increase in R_a stops at $T = 1000$ K.

DISCUSSION OF RESULTS

The real mode of variation in the state of a fluid can lead to its overheating over the boiling point. A fluid is overheated either due to fast heating at a constant pressure or due to fast depressurizing at a constant temperature. In any case, the fluid passes to the metastable state in which its temperature is higher than the boiling temperature at normal pressure. The degree of such overheating for nonmetallic fluids can reach hundreds of degrees and depends mainly on the heating or depressurizing rate. In the limiting case of the full absence of vapor, an amazingly high degree of overheating can be reached. The release of overheating proceeds as an instantaneous change in the phase in the form of explosive ebullience. The process limiting the high overheating of a fluid is homogeneous nucleation. The limiting overheating of water is 329–333 K [28, 29]. In this case, according to the estimate of [30], the critical nucleus contained about 20 molecules.

Phase transitions in metallic systems have certain specificities. The situation is that, in this case, electron and molecular structures of equilibrium liquid and vapor phases differ strongly. For example, liquid mercury and cesium near their ordinary melting points are considered normal liquid metals with properties typical of the condensed state. Small variations in their basic properties such as electrical conductivity or magnetic susceptibility on melting show that the electron structure of the liquid is similar to the structure of a crystalline solid. Such a behavior is usually explained by the fact that short-range atomic correlations in a small volume of the liquid and crystal are similar. In additions, ion charges in metals are well-screened by conduction electrons; therefore, the long-range order in ionic potentials is important neither for a liquid nor for a solid. An illustrious example of the unusual behavior of the metallic system is the metal–nonmetal transition upon evaporation of a dense liquid. The low surface free energy of most nonmetallic bodies excludes their wetting by inert (unreactive) liquid metals. However, for mercury on glass, quartz, and sapphire, there exists a preliminary-wetting transition. The presence of the metal–nonmetal transition appreciably influences the thermodynamic, structural, interphase, and dynamic features of metals. The dependences of the conductivity on density for bivalent mercury can be divided into three regions.

Mercury is a polyvalent metal, available for study in the liquid state. The critical point for vapor is characterized by the following parameters: $T_c = 1751$ K, $p_c = 167.3$ MPa, and $\rho_c = 5.8$ g/cm^3. It is the lowest known critical temperature of liquid metals. This fact is important for measuring the physical properties at high temperatures and pressures.

The results of a number of experiments on evaporation of drops from a hot surface point out the existence of a discontinuity in the dependence of the temperature difference $\Delta T = T^i_{\text{vap}} - T^i_{\text{liq}}$ (i means interface) on the vapor pressure p^i_{vap} [31, 32]. In the liquid–vapor interface, the temperature is always higher from the side of vapor. The reason is that molecules with the highest energy evaporate in the first instance and less energetic molecules remain in the drop. The reduction in the molecular flux to the vapor phase is observed mainly at high temperatures; for water $T/T_c \approx 0.84$ [33]. The temperature jump for water can be higher than 1400 K [33]. The surface tension of mercury (0.46 J/m^2) is higher than that of water (0.0729 J/m^2). Mercury atoms are 11 times heavier than water molecules. The type of interaction in mercury is different. It may be assumed that a mercury drop preserves its stability at high temperatures due to the reduction in the Hg atom flux to the vapor phase but the features of this process are different from the behavior of water. The destruction of Stone–Wales defects upon heating of graphene is mainly due to the vertical displacement of C atoms, which is indicated by the increase in roughness. The vertically moving C atoms hit Hg atoms of the drop and push it upward.

The high stability of the mercury drop in the model can also be explained by the following circumstance. The potential of interaction between two mercury atoms, as a rule, is considered a potential between strongly polarizable closed shells admitting only a small migration of the electron density; i.e., to a certain extent, it is similar to the potential function describing the interaction between noble gas atoms. Mercury drop formation on graphene upon fast heating was also confirmed by a similar calculation with the SG-potential for representing the Hg–Hg interactions [34]. A Hg film upon heating contracted into a drop. Toward the end of the calculation, at 600 K, a spherical drop on graphene was formed and, at 800 K, the drop detached from graphene. However, in contrast to the calculations with the Sch-potential, the use of the SG-potential function slowly increased the distance between the drop and graphene up to the temperature of 1100 K. Most likely, the increased stability of the mercury drop means that the SG- and Sch-potentials overestimate the indirect influence of the electron component on the Hg–Hg interaction.

In three-dimensional semiconductors (diamond, silicon, germanium), natural point defects are vacancies, interstices, substitutional impurities, and their complexes, while, in graphene, it is the Stone–Wales defect. The quantum mechanical computation has revealed that plastic tensile strain in graphene can lead to the formation of SW defects [35]. After forming the SW defect, the graphene sheet does not remain in the plane. Two atoms of the rotated C–C-bond move perpendicularly to the monolayer plane by ~0.3 Å in the opposite direction, entraining other nearby atoms, which increase the difference between transverse displacements [36]. As a result, a sinusoidal distortion of the monolayer arises. This process is enhanced upon heating of graphene. In this case, a significant increase in roughness is observed, and, on larger sheets, corrugation is formed.

CONCLUSIONS

Stepwise heating of mercury film on imperfect graphene has been studied by the molecular-dynamic method. A graphene sheet with a high concentration of Stone–Wales defects and hydrogenated edges was studied. An increase in temperature led to a gradual transformation of the film into a drop, followed by the detachment of the drop from graphene. The horizontal component of the Hg atom mobility smoothly decreases during the process, and the vertical component, after a decrease reached at the temperature of 600 K, nonmonotonically increased. As a whole, the spectra of horizontal and vertical vibrations of Hg atoms vary with temperature in a similar manner: small-scale fluctuations caused by temperature changes in the spectra are smoothed. The vertical profile of the density of mercury shifts upward and expands to the size corresponding to the diameter of the liquid metal drop having formed. The mercury drop formation is accompanied with a contraction of the range of significant values of the radial distribution function and a reduction in the number and intensities of pronounced peaks of $g(r)$. An increase in temperature causes changes in the metric properties of graphene with defects. In the angular distribution of the nearest neighbors, the intensity of the main peak at 120°, produced by hexagonal cells, decreases and intense peaks corresponding to the angles of 30°, 90°, and 150° appeared. At all temperatures, the stresses in the graphene plane, caused by the vertical forces, exceed the stresses produced by horizontal forces. Most often, this excess is multifold. The roughness of graphene rapidly increases with temperature and reaches the maximum at 1000 K. In the high-temperature region, the hydrogenated edges of graphene were slightly damaged. Thus, to a great extent, the possibility to use heating to clean graphene of mercury is determined by the presence of the Stone–Wales defects in it.

ACKNOWLEDGMENTS

This work was supported by the Russian Foundation for Basic Research, project no. 13-08-00273.

REFERENCES

1. Galashev, A.E. and Rakhmanova, O.R., *Phys.–Usp.*, 2014, vol. 57, no. 10, p. 970.
2. Valota, A.T., Kinloch, I.A., Novoselov, K.S., Casiraghi, C., Eckmann, A., Hill, E.W., and Dryfe, R.A.W., *2D Mater.*, 2015, vol. 2, 024011. http://dx.doi.org/10.1088/2053-1583/2/2/024011
3. Velicky, M., Bradley, D.F., Cooper, A.J., Hill, E.W., Kinloch, I.A., Mishchenko, A., Novoselov, K.S., Patten, H.V., Toth, P.S., Valota, A.T., Worrall, S.D., and Dryfe, R.A.W., *ACS Nano*, 2014, vol. 8, p. 10089.
4. Lee, C.W., Serre, S.D., Zhao, Y., Lee, S.J., and Hastings, T.W., *J. Air Waste Manage. Assoc.*, 2008, vol. 58, p. 484.
5. Huggins, F.E., Yap, N., Huffman, G.P., and Senior, C.L., *Fuel Process. Technol.*, 2003, vol. 82, p. 167.
6. Hutson, N.D., Attwood, B.C., and Scheckel, K.G., *Environ. Sci. Technol.*, 2007, vol. 41, p. 1747.
7. Wilcox, J., Sasmaz, E., and Kirchofer, A., *J. Air Waste Manage. Assoc.*, 2011, vol. 61, p. 418.
8. Azamat, J., Khataee, A., and Joo, S.W., *J. Mol. Graphics Modell.*, 2014, vol. 53, p. 112.
9. Kim, H.W., Yoon, H.W., Yoon, S.-M., Yoo, B.M., Ahn, B.K., Cho, Y.H., Shin, H.J., Yang, H., Paik, U., Kwon, S., Choi, J.-Y., and Park, H.B., *Science*, 2013, vol. 342, p. 91.
10. Galashev, A.E. and Polukhin, V.A., *Phys. Met. Metallogr.*, 2014, vol. 115, no. 7, p. 697.
11. Galashev, A.E. and Rakhmanova, O.R., *High Temp.*, 2014, vol. 52, no. 3, p. 374.
12. Galashev, A.E., *High Temp.*, 2014, vol. 52, no. 5, p. 633.
13. Orekhov, N.D. and Stegailov, V.V., *High Temp.*, 2014, vol. 52, no. 2, p. 198.
14. Zakharchenko, K.V. and Fasolino, A., Los, J.H., and Katsnelson, M.I., *J. Phys.: Condens. Matter*, 2011, vol. 23, p. 202202.
15. Tersoff, J., *Phys. Rev. Lett.*, 1988, vol. 61, p. 2879.
16. Burgos, E., Halac, E., and Bonadeo, H., *Chem. Phys. Lett.*, 1998, vol. 298, nos. 4–6, p. 273.
17. Stuart, S.J., Tutein, A.V., and Harrison, J.A., *J. Chem. Phys.*, 2000, vol. 112, p. 6472.
18. Galashev, A.E. and Polukhin, V.A., *Phys. Solid State*, 2013, vol. 55, no. 8, p. 1733.
19. Schwerdtfeger, P., Wesendrup, R., Moyano, G.E., Sadlej, A.J., Greif, J., and Hensel, F., *J. Chem. Phys.*, 2001, vol. 115, p. 7401.
20. Kutana, A. and Giapis, K.P., *Nano Lett.*, 2006, vol. 6, p. 656.
21. Silvera, I.F. and Goldman, V.V., *J. Chem. Phys.*, 1978, vol. 69, p. 4209.
22. Lamari, F.D. and Levesque, D., *Carbone*, 2011, vol. 49, p. 5196.
23. Verlet, L., *Phys. Rev.*, 1967, vol. 159, p. 98.
24. Berendsen, H.J.C., Postma, J.P.M., van Gunsteren, W.F., DiNola, A., and Haak, J.R., *J. Chem. Phys.*, 1984, vol. 81, p. 3684.
25. Hafskjold, B. and Ikeshoji, T., *Phys. Rev. E: Stat., Nonlinear, Soft Matter Phys.*, 2002, vol. 66, no. 1, p. 011203.
26. Davydov, S.Yu., *Phys. Solid State*, 2012, vol. 54, no. 4, p. 875.
27. Rao, R.V.G. and Murthy, A.K.K., *Phys. Status Solidi B*, 1974, vol. 66, p. 703.
28. Eberhart, J.G. and Pinks, V., *J. Colloid Interface Sci.*, 1985, vol. 7, p. 574.
29. Salla, J.M., Demichela, M., and Casal, J., *J. Loss Prev. Process Ind.*, 2006, vol. 19, p. 690700.
30. Monde, M. and Hasan, M.N., in *Proc. Int. Conf. on Mechanical Engineering 2011 (ICME2011)*, Dhaka: BUET, 2011, p. KEY-004.
31. Ward, C.A. and Stanga, D., *Phys. Rev. E: Stat., Nonlinear, Soft Matter Phys.*, 2001, vol. 64, p. 051509.
32. McGaugheya, A.J.H. and Ward, C.A., *J. Appl. Phys.*, 2002, vol. 91, p. 6406.
33. Lotfi, A., Vrabec, J., and Fischer, J., *Int. J. Heat Mass Transfer*, 2014, vol. 73, p. 303.
34. Galashev, A.E., *Colloid J.*, 2015, vol. 77, no. 5, p. 582.
35. Orlikowski, D., Nardelli, M.B., Bernholc, J., and Roland, C., *Phys. Rev. B: Condens. Matter Mater. Phys.*, 2000, vol. 61, p. 14194.
36. Ma, J., Alfe, D., Michaelides, A., and Wang, E., *Phys. Rev. B: Condens. Matter Mater. Phys.*, 2009, vol. 80, p. 033407.

Translated by E. Chernokozhin